

1 **Numerical investigation of TiO₂ and MWCNTs turbine meter oil**
2 **nanofluids: Flow and hydrodynamic properties**

3 Atiyeh Aghaei Sarvari^a, Saeed Zeinali Heris^{a,*}, Mousa Mohammadpourfard^a, Seyed
4 Borhan Mousavi^b, Patrice Estellé^c

5 ^a Faculty of Chemical and Petroleum Engineering, University of Tabriz, Tabriz, Iran

6 ^b Department of Mechanical Engineering, University of British Columbia, Vancouver,
7 BC, Canada

8 ^c Univ Rennes, LGCGM, EA3913, F-35000 Rennes, France

9 *Corresponding Author Email: s.zeinali@tabrizu.ac.ir

10 **Abstract**

11 The main aim of the present study is to evaluate the influence of multi-walled carbon
12 nanotubes (MWCNTs) and TiO₂ nanoparticles (NPs) on lubricant and fluid flow within natural
13 gas turbine meters. In light of this purpose, disparate concentration of TiO₂ NPs (0.1, 0.2, and
14 0.3 wt%), various volume flow rates 0.14, 0.35, and $0.12 \frac{cm^3}{s}$ were employed for experimental
15 analyses. In the facet of simulation, Gambit software version 2. 4. 6 to mesh oil pathway and
16 Fluent software version for solving the equations were utilized. It was revealed that the pressure
17 drop in the presence of nanoparticles was increased. Moreover, there was an increase in
18 pressure drop value with raising the NPs concentration; for instance, the pressure drop value
19 of MWCNTs-containing nanofluids at the volume flow rate of 0.35 cm enhanced from 92.72
20 Pa to 94.64 Pa as the NPs concentration raised from 0.1 to 0.3. Furthermore, modeling
21 outcomes corroborated the uptrend in pressure drop value by increasing the volume flow rate
22 and reported the maximum pressure drop value of $0.12 \frac{cm^3}{s}$. On the other hand, the numerical
23 results revealed that the friction coefficient is directly and inversely proportional to NPs

24 concentration and the volume flow rates, sequentially. Additionally, with increasing the
25 volume flow rate, the entrance length increased, and reaching the developed state was delayed.
26 It is worth noting as the final finding of this study that increasing the NPs concentration resulted
27 in decreasing the entrance length and the fast reaching of the developed state.

28 **Keywords:** Nanofluid; Lubricant; MWCNTs; TiO₂ nanoparticles; Gas turbine-meter; Pressure
29 drop.

30 **Nomenclature**

31 Q Flow rate ($\text{m}^3 \text{s}^{-1}$)
32 U Velocity (m s^{-1})
33 A Cross-section area (m^2)
34 K Local energy dissipation coefficient
35 g Gravitational acceleration ($\text{m}^2 \text{s}^{-1}$)
36 Re Reynolds number
37 L Length (m)
38 wt Nanoparticle weight fraction (%)
39 D Diameter (m)
40 P Pressure ($\text{kg m}^{-1} \text{s}^{-2}$)
41 F Coefficient of friction

42 **Greek letters**

43 μ Kinematic viscosity ($\text{mm}^2 \text{s}^{-1}$)
44 ρ Density (kg m^{-3})

45 **Subscripts**

46 e Entrance

47 nf Nanofluid

48 bf Base fluid

49 **1. Introduction**

50 Tribology is the science of control and handling of wear, friction, and lubrication.
51 Lubrication is a method of preventing friction and abrasion of moving surfaces that lump
52 together. The friction is undesirable in most machines, so it is always attempted to be reduced
53 or eliminated. Friction also causes erosion, noise, reducing durability, and heat generation of
54 the equipment. Loss of energy is the most significant problem caused by wear and friction [1,
55 2]. Good lubricant quality is required to reduce friction and improve the performance of parts
56 of a machine or surfaces that are in contact with each other. Since most oils cannot be used
57 directly or purely, they are mixed with certain additives to improve their viscosity and
58 properties, most of which are nanomaterials [3-6]. Nanoparticles can enhance the tribological
59 and anti-wear characteristics of oils by one of the following mechanisms (1) rolling effect,
60 which can occur in the presence of small spherical nanoparticles rolling between the two
61 contacting surfaces altering the sliding friction to rolling friction, (2) in the mending effect the
62 mass loss will be compensated due to the incorporation of nanoparticles from the physical film,
63 (3) nanoparticles polish the contact surface and decrease the surface roughness, and (4)
64 nanoparticles protect the contacting surfaces by providing a stable tribo-film [7]. Nano
65 lubricants are mainly used in the turbine meter to reduce friction and wear in bearings. Most
66 turbine meters are equipped with a lubrication system that changes the oil pump's size based
67 on the turbine meter's capacity. Constant lubrication of the turbine meter is required to achieve
68 a longer service life.

69 Carbon nanotubes (MWCNTs) have attracted attention due to their remarkable properties,
70 such as small size, high surface density, and weak covalent bonds, leading the plates to slip on

71 each other, reducing the friction of the contact plates in the lubrication system [8-13]. In
72 addition, MWCNTs/nanofluid has excellent physicochemical and heat transfer properties viz.
73 thermal conductivity, high thermal stability, high viscosity index, low pour point, and high
74 flash point [14-23].

75 Titanium dioxide (TiO_2) nanoparticles are used in many industries because of their excellent
76 heat transfer, lubricity, optical, electrical, and catalytic properties. These applications include
77 industrial pigments, environmental clean-up photocatalysts, skin protectors in sunscreens, and
78 lubricants as additives [24-29]. Many investigations have shown the anti-friction
79 characteristics of TiO_2 nanoparticles due to their inherent anti-friction functionality, ease of
80 synthesis, and low toxicity [30-33].

81 Different parameters of nanoparticles such as structure, functional surface groups, and
82 concentrations affect the tribological properties of lubricants. The shape of the nanoparticles is
83 another crucial parameter; the nanospheres experience more pressure at a given load than the
84 nanoparticles because the former contact surface area is much smaller. Therefore, using layer
85 nanoparticles can minimize the deformation of the wear surfaces [34-38]. Studies have shown
86 that even a small concentration of nanoparticles can effectively improve the tribological
87 properties. However, all the operating system parameters must be considered to find the
88 optimum concentration for the minimum coefficient of friction [39-42]. Numerous studies have
89 been conducted to investigate the effect of TiO_2 nanoparticles and MWCNTs on the
90 tribological properties of base fluid, which in most cases improved the performance of the
91 lubricants and oils [43-50].

92 Heris et al. [51] investigated the thermal conductivity of turbine oil-based nanofluids inside
93 a circular tube under laminar flow and constant flow rate. Three different nanofluids were
94 prepared using TiO_2 , CuO , and Al_2O_3 nanoparticles at different concentrations. The results
95 showed an increase in heat transfer coefficient and Nusselt number with the addition of

96 nanoparticles. They also introduced a parameter as the ratio of nanofluid pressure drop to base
97 fluid pressure drop and observed that this parameter was always greater than one. In other
98 words, the addition of nanoparticles increased the pressure drop. Hosseinzadeh et al. [52]
99 evaluated the effect of magnetic field and nanoparticle concentrations on heat transfer
100 coefficient and friction in the presence of water and Fe_3O_4 nanoparticles. The experiments were
101 performed inside a horizontal tube with a diameter of 7 mm and a length of 1 meter in different
102 Reynolds numbers. The results showed that the Nusselt number increased with the addition of
103 nanoparticles and Reynolds numbers. Additionally, the same result was observed with
104 increasing magnetic field strength. The presence of nanoparticles increased the coefficient of
105 friction but increasing the intensity of the magnetic field had no significant effect on the
106 coefficient of friction. Furthermore, increasing the Reynolds number decreased the coefficient
107 of friction. Ahmad Ali et al. [53] conducted a study to assess the effect of TiO_2 and Al_2O_3
108 nanoparticles on the thermophysical and tribological characteristics of engine oil. The
109 outcomes revealed that the coefficient of friction decreased by 40~50% and the tire wear rate
110 decreased by 20~30%. They concluded that adding nanoparticles could remarkably enhance
111 the thermophysical and tribological properties of engine oil. Borda et al. [54] examined the
112 effect of Cu nanoparticles on mineralized and synthesized oil-based esters considering different
113 concentrations. Their findings exhibited that the addition of Cu nanoparticles did not have a
114 good effect on friction and wear on the synthesized oil. However, adding these nanoparticles
115 to mineral oil decreased the coefficient of friction and improved the wear properties, especially
116 at 0.3 wt% of the nanoparticles. Laad et al. [55] added TiO_2 nanoparticles to improve the
117 lubricating oil properties. Nanofluids were prepared at different concentrations, 0.3, 0.4, and
118 0.5 wt%. A pin-on-disc tribometer was used to perform abrasion and friction tests. The results
119 showed that the coefficient of friction increased with increasing the nanoparticles
120 concentration. They asserted that the addition of this nanoparticle could reduce the amount of

121 wear and coefficient of friction and improve the lubricant properties. Curà et al. [56] studied
122 the effect of graphene nanoplates on the tribological performance of lubricants considering
123 different concentrations. It was observed that the addition of the used nanoparticles could
124 significantly improve the tribological features of the lubricants. Hussein et al. [57]
125 experimentally examined the effect of MWCNT/water nanofluids on heat transfer attributes
126 and pressure drop at diverse concentrations ranging from 0.075–0.25 wt%. The experiments
127 were conducted inside a circular mini tube under a laminar flow condition. The results showed
128 that as the nanoparticle concentration increased, the coefficient of friction, the coefficient of
129 heat transfer, and pressure drop increased. A 10% increase in pressure drop was reported at the
130 highest concentration of nanoparticles. The effect of adding MWCNTs and graphene
131 nanoplatelets on the thermal properties of the diesel oil at different concentrations and flow
132 rates were assessed by Naddaf et al. [58]. The outcomes confirmed that the thermal properties
133 of the prepared nanofluids were dependent on the concentration of nanoparticles. They further
134 reported that both the convective heat transfer coefficient and the pressure drop increased with
135 the addition of nanoparticles. Mousavi et al. [59] investigated the thermophysical and
136 rheological properties of MoS₂/diesel oil-based nano lubricants. A pin-on-disc friction and
137 wear tester was employed to evaluate the friction and anti-wear properties. The highest
138 viscosity and viscosity index were observed at the highest concentration in the study, 0.7 wt%.
139 Ajeel et al. [60] evaluated the simultaneous effect of corrugated walls and turbulent flow of
140 nanofluids on thermohydraulic performance. The experiments were conducted at diverse
141 Reynolds numbers ranging in 10,000–30,000 and a heat flux of $10000 \frac{W}{m^2K}$. Three different
142 channel shapes were considered as a semicircular, wavy channel, trapezoidal wavy channel,
143 and straight channel. The nanofluids were prepared in volumetric percentages of 1% and 2%
144 of Al₂O₃. The results showed that the nanofluid flow inside the trapezoidal corrugated channel
145 increased 63.54% of the heat transfer coefficient and 1.37 times the pressure drop compared to

146 the straight channel. Pourpasha et al. [61] assessed the effect of CNT on the thermophysical
147 and tribological features of turbine oil meter nano lubricants. The thermophysical properties of
148 lubricating oil such as viscosity index, kinematic viscosity, flash point, pressure drop, and
149 coefficient of friction were measured. It was found that the addition of CNT could enhance
150 lubrication characteristics and improve the thermophysical of the turbine meter oil nano
151 lubricants.

152 Based on the performed literature survey, most studies in the field of heat transfer
153 characteristics of nano lubricants announce a positive effect on the friction-reduction behavior
154 and thermophysical characteristics considering different nano additives. However, in the
155 previous investigations, none of the studies were conducted while considering TiO₂ and
156 MWCNTs nanoparticles in the turbine meter oil. Furthermore, heat transfer characteristics and
157 tribological behaviors of the TiO₂ and MWCNTs nano lubricants have not been well-
158 understood. It is worth mentioning that different effective parameters such as concentration of
159 nanoparticles, flow rates, and pressure drops were comprehensively studied in this study.

160 In this study, to the best of our knowledge, lubrication oil simulation has been measured
161 inside the turbine for the first time. The velocity profiles, pressure drop values, coefficient of
162 friction of the base fluid, and nano lubricants considering MWCNTs and TiO₂ nanoparticles
163 considering different weight percentages and volume flow rates were comprehensively
164 investigated.

165 **2. Experimental Section**

166 **2.1. Materials**

167 Table 1 lists the specifications of the gas turbine meter oil manufactured by Shell Oil
168 Company, USA. The TiO₂ and MWCNTs were commercially purchased from SkySpring
169 Nanomaterials, USA, and US Research Nanomaterials, USA, respectively. These data were

170 reported by Pourpasha et al. [61]. Table 2 represents the specifications of the used
171 nanomaterials. Figures 1 and 2 represent the SEM images of TiO₂ nanoparticles and MWCNTs,
172 respectively. The specification of nanofluids is listed in Table 3.

173

174

Table 1 Specifications of gas turbine meter oil.

Properties	Unit	ASTM standard	Value
Density	Kg/m ³	D1298	775
Viscosity at 40°C	cSt	D445	21.88
Viscosity at 100°C	cSt	D445	4.6
Viscosity index (VI)	–	D2270	130
Pour point	°C	D97	–40
Flash point	°C	D92	220

175

Table 2 Physical properties of nanoparticles.

Nanoparticles	Morphology	Purity (%)	Average diameter (nm)	Density (kg/m ³)	Color
TiO ₂	Spherical	99.5	10	4230	White
MWCNTs	Cylindrical	>95	13	2100	Black/Gray

176

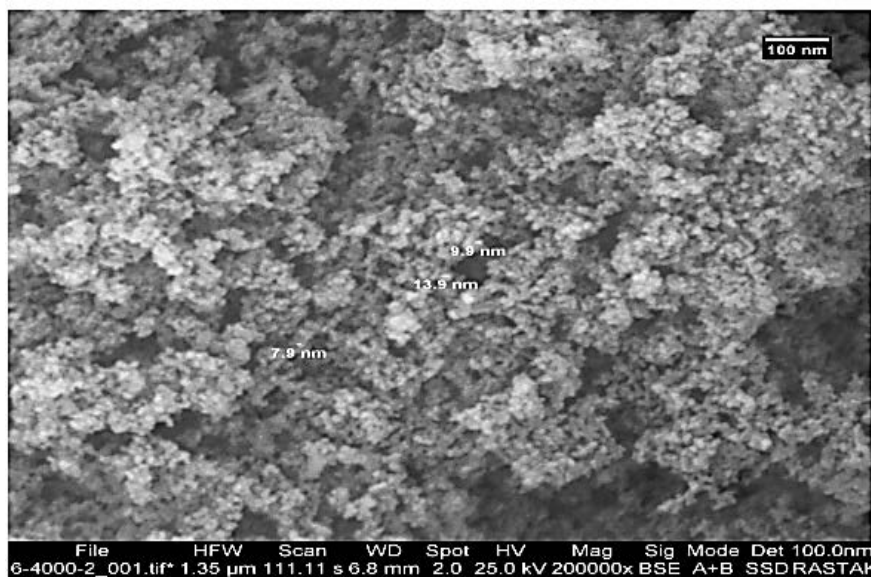


Fig. 1. SEM image of TiO_2 nanoparticles.

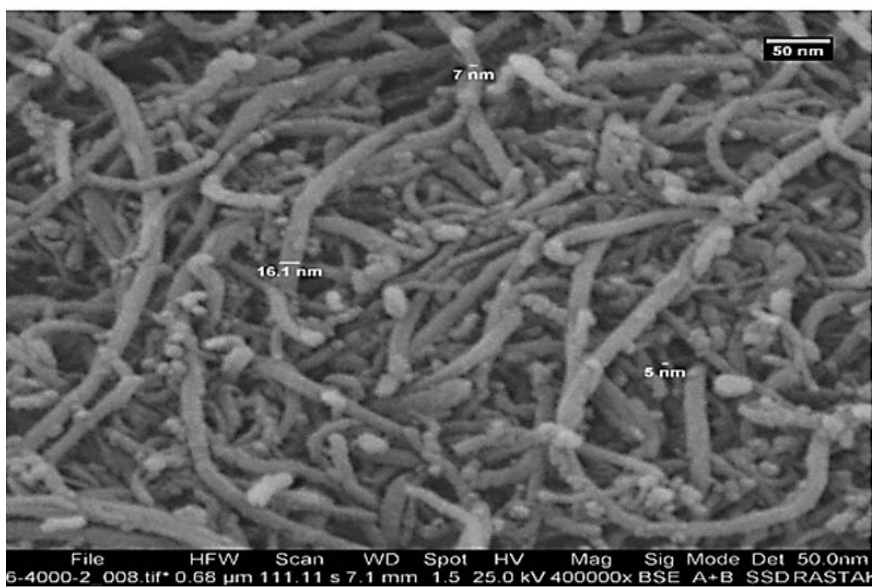


Fig. 2. SEM image of MWCNTs.

Table 3 Specifications of nanofluids.

Nanofluid	Density (kg/m ³)	Viscosity at 40°C (cSt)
0 (Base oil)	775	21.88
0.1 wt% TiO ₂	776	21.407
0.2 wt% TiO ₂	776.4	21.645
0.3 wt% TiO ₂	777	21.826
0.1 wt% MWCNTs	775.8	21.651
0.2 wt% MWCNTs	776.4	21.852
0.3 wt% MWCNTs	777	22.071

184 2.2. Methods for experiment

185 The velocity inlet is essential information needed for modeling nanofluid flow through the
 186 gas turbine meter conduit. The oil pathway and the pump were used to measure the velocity.
 187 Figure 3 shows the oil inlet pathway for the velocity measurement system. A certain amount
 188 of oil was pumped through the oil pump to the oil pathway to measure inlet velocity. The inlet
 189 velocity was determined by measuring the time to complete oil outflow using equation 1.

$$Q = U \times A \quad (1)$$

190 where Q is the volume flow rate (m³/s), U is the velocity (m/s), and A is the cross-sectional
 191 area (m²).



192

193

Fig. 3. Turbine meter oil inlet pathway for the velocity measurement system.

194

2.3. The pressure drops from theoretical relationships

195

Two types of energy loss for pipes can be considered: first is the loss due to the change in the diameter of the pipes and the types of joints (minor loss). Second is the loss due to friction in the pipes (major loss), higher than the other. Factors such as changing the diameter of the pipes and the existence of different types of joints (knees, valves, and curvature in the pipes.) cause the deformation of the flow lines resulting in energy loss. The following formula can calculate this type of loss [62]:

196

$$h_f = K \frac{U^2}{g} \quad (2)$$

197

198

199

200

$$\Delta P = \rho g h_f \quad (3)$$

201

In the above relation, K is the local energy dissipation coefficient (the empirical coefficient obtained from the corresponding tables without dimension), U is the velocity (m/s) (the inlet

202

203 velocity), ΔP is the pressure drop (Pa), ρ as density (kg/m^3), and g is the gravitational
204 acceleration (m^2/s).

205 Depending on the shape and geometry, this type of pressure loss involves a pressure drop
206 caused by the presence of a knee and a sudden change in the cross-sectional area. The
207 coefficient of local energy loss resulting from the cross-sectional area change can be obtained
208 from equation 4 [63]:

$$K = \left(1 - \frac{A_1}{A_2}\right)^2 \quad (4)$$

209 where A_1 is a small cross-section and A_2 is a large cross-section.

210 The simulation has been performed at a constant temperature without heat transfer, steady-
211 state condition, and under the laminar flow condition. The frictional pressure drop is dependent
212 on the friction between the fluid and the pipe, which is shown for a circular pipe with the
213 Darcy-Weisbach relation.

$$\Delta P = F_D \times \frac{\rho L}{2} \times \frac{U^2}{D} \quad (5)$$

$$F_D = \frac{64}{Re} \quad (6)$$

$$Re = \frac{\rho U D}{\mu} \quad (7)$$

214 Where ΔP is pressure drop [Pa], F_D is coefficient of friction, D is diameter [m], L length of
215 pipe [m], ρ is density [kg/m^3], U is velocity [m/s], and μ is viscosity [kg/m.s].

216 **2.4. Developing entrance length and developed flow and theoretical relationships**

217 For laminar flow, the hydrodynamic entrance length can be obtained from the following
218 equation [64]:

219 $\frac{l_e}{D} = 0.058 Re$ (8)

220 where l_e is the entrance length and D is the diameter of the pipe.

221 3. Numerical simulation

222 3.1. Simulation of nanofluids

223 As mentioned, this study aims to simulate the flow of nanofluids inside the oil pathway.
224 Single-phase and general two-phase methods are used to model the flows involving
225 nanoparticles. In the two-phase approach, nanofluids are considered two different liquid and
226 solid phases with different momentums. The equations resulting from the two-phase theory are
227 difficult to deal with and cannot be easily applied for nanofluids. In the single-phase approach,
228 both the fluid phase and nanoparticles are considered a single homogeneous phase. Since the
229 particles are ultrafine and become easily fluidized, all the equations of continuity, motion, and
230 energy for pure fluid may be directly extended to nanofluids. In this study, due to the low
231 concentration of nanoparticles and the experimental determination of properties such as
232 viscosity and density, the homogeneous model has been used to simulate the nanofluid flow
233 through the gas-turbine oil meter path.

234 3.2. Governing Equations

235 The pressure drop is obtained from the continuity and momentum balance equations.
236 Equations 5, 7, and 8 represent these equations.

$$\frac{\partial \rho}{\partial t} + \nabla \cdot (\rho \vec{v}) = 0 \quad (7)$$

$$\frac{\partial}{\partial t} (\rho \vec{v}) + \nabla \cdot (\rho \vec{v} \vec{v}) = -\nabla P + \nabla \tau + \rho \vec{g} + \vec{F} \quad (8)$$

$$\frac{\Delta P}{L} = F_D * \frac{\rho}{2} * \frac{V^2}{D} \quad (9)$$

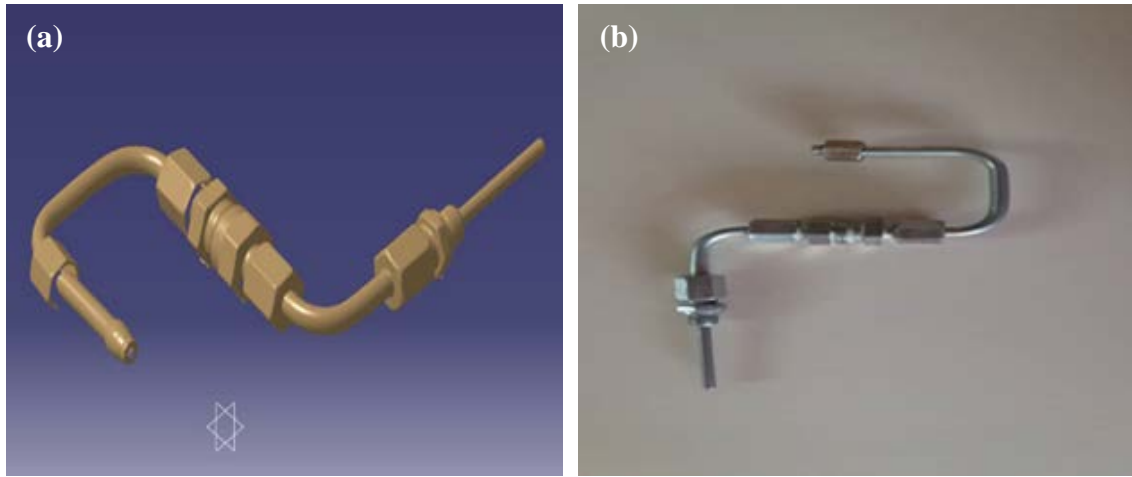
237 where P is the static pressure, ΔP is a pressure drop, $\rho \vec{g}$ and \vec{F} are the gravitational body
238 force and exterior body forces, F_D is coefficient of friction, and D is diameter [63].

239 In the homogeneous model, the thermophysical properties of nanofluid such as viscosity
240 and density must be used in continuity, momentum, and energy equations.

241 In the present study, experimental values of viscosity and density are given by Pourpasha et
242 al. [61] were used in the continuity and momentum equations.

243 3.3. Boundary conditions and needed information

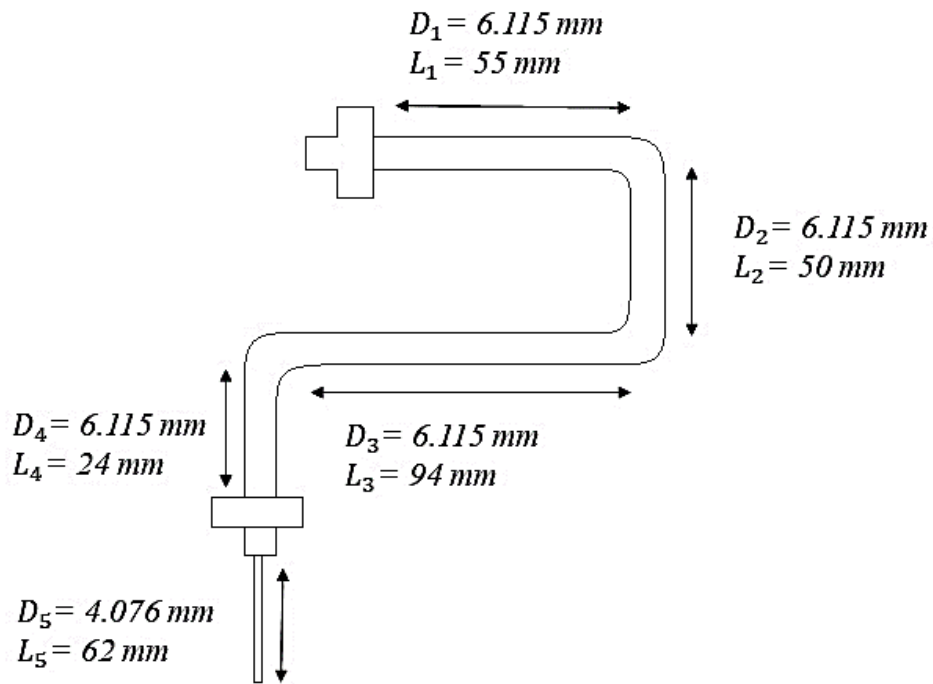
244 The purpose of this present study is to investigate the effect of MWCNTs and TiO₂
245 nanoparticles on the modeling of lubricant fluid flow within gas turbine meters. A lubrication
246 system is necessary due to the high degree of wear and coefficient of friction of the bearings.
247 In this regard, the lubricating oil pathway inside the gas turbine meters has been investigated
248 and simulated. The CMM scanner scans the oil path in figure 4.. The condition used as the
249 boundary condition is the inlet velocity is 0.00483, 0.0409, and 0.012 (m/s). The dimension of
250 the oil pathway is shown in figure 5. The oil pathway from part 1 to part 4 is iron, and part 5 is
251 steel. The simulation is performed at a constant temperature without heat transfer, steady-state
252 condition, and under the laminar flow condition.



253

254

Fig. 4. (a) Scanned and (b) the real photo of the turbine meter oil pathway.



255

256

Fig. 5. Dimension of oil pathway.

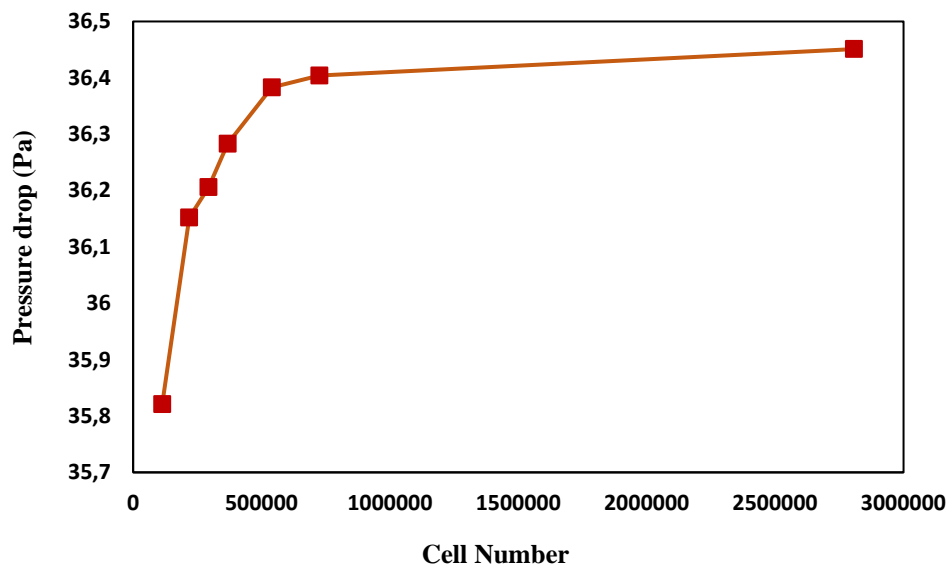
257 3.4. Numerical Analysis

258 The oil pathway is meshed by Gambit software version 2. 4. 6 and the equations have been

259 solved by Fluent software version 19.1. ANSYS-FLUENT software has been used to solve the

260 governing equations discretized with a double-precision solver using the SIMPLEC algorithm.
261 The convergence criteria for continuity, momentum, and energy equations were all set to 10^{-6} .

262 For the mesh independence check, figure 6 is plotted, and given the optimal number of
263 cells, 368462 is selected. The absolute convergence criteria for the continuum equation and the
264 velocity equation with residuals below have been considered.



265

266 **Fig. 6.** Pressure drop variations versus cell number.

267 **4. Results**

268 **4.1. Results of TiO₂/turbine meter oil nanofluids**

269 This section discusses the effect of increasing volume flow rate and mass percent of
270 nanoparticles on pressure drop, coefficient of friction, and velocity profile. Furthermore, the
271 effect of simultaneous mass percent of nanoparticles and volume flow rate on pressure drop
272 and coefficient of friction are discussed. Different results are presented in Table 4 to compare
273 the outlet velocity of the simulation and the theoretical relationships. The differences between
274 experimental and numerical values of outlet velocities are 2.48%, emphasizing the accuracy

275 and correctness of the numerical simulation. Table 5 lists the pressure drop values of
 276 TiO₂/turbine meter oil nanofluid at volume flow rates of 0.14, 0.35, and 1.2 $\frac{cm^3}{s}$. Figure 7 shows
 277 the effect of TiO₂ concentration on the pressure drop variations as a function of flow rate.

278 **Table 4** The velocity values of modeling and theoretical relationships.

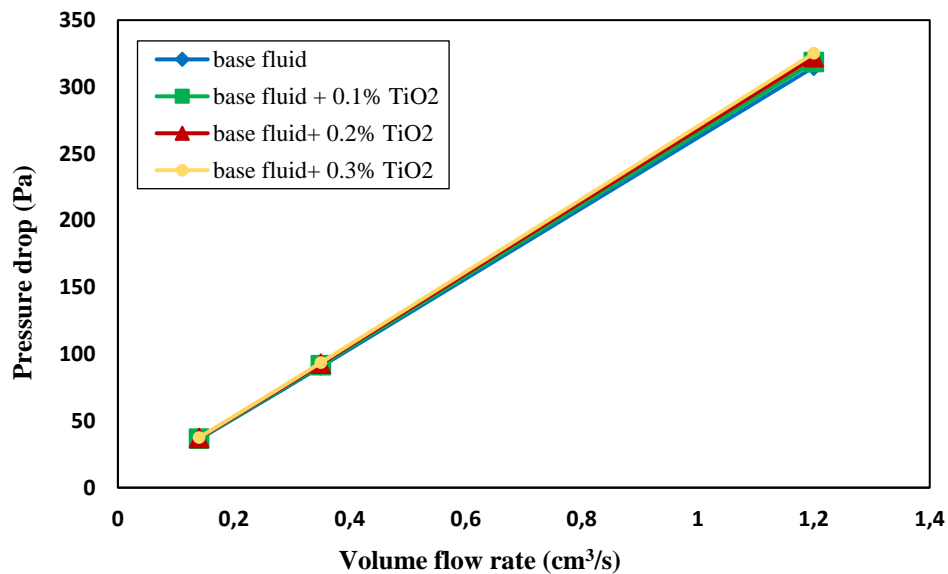
Fluid	Inlet velocity (m/s)	Modeling outlet velocity (m/s)	Theoretical outlet velocity (m/s)	Difference (%)
Base oil	0.00483	0.0106	0.01087	2.48

279

280 **Table 5** Modeling and theoretical pressure drop values of TiO₂ nanofluids at different flow rates.

Concentration (wt%)	Flow rate ($\frac{cm^3}{s}$)	Modeling pressure drop (Pa)	Theoretical pressure drop (Pa)	Difference (%)
0 (base oil)	0.14	36.28	36.44	0.439
	0.35	90.59	90.64	0.055
	1.2	314.91	310.74	1.342
0.1 TiO ₂	0.14	36.73	36.90	0.461
	0.35	91.68	92.60	0.994
	1.2	318.65	313.17	1.750
0.2 TiO ₂	0.14	37.15	37.31	0.429
	0.35	92.72	93.08	0.387
	1.2	322.20	316.80	1.705
0.3 TiO ₂	0.14	37.50	37.67	0.451
	0.35	93.60	93.62	0.021
	1.2	325.19	319.81	1.682

281



282

283 **Fig. 7.** The effect of TiO₂ concentration on the pressure drop variations as a function of flow rate.

284

285

286

287

288

289

290

291

292

293

294

295

296

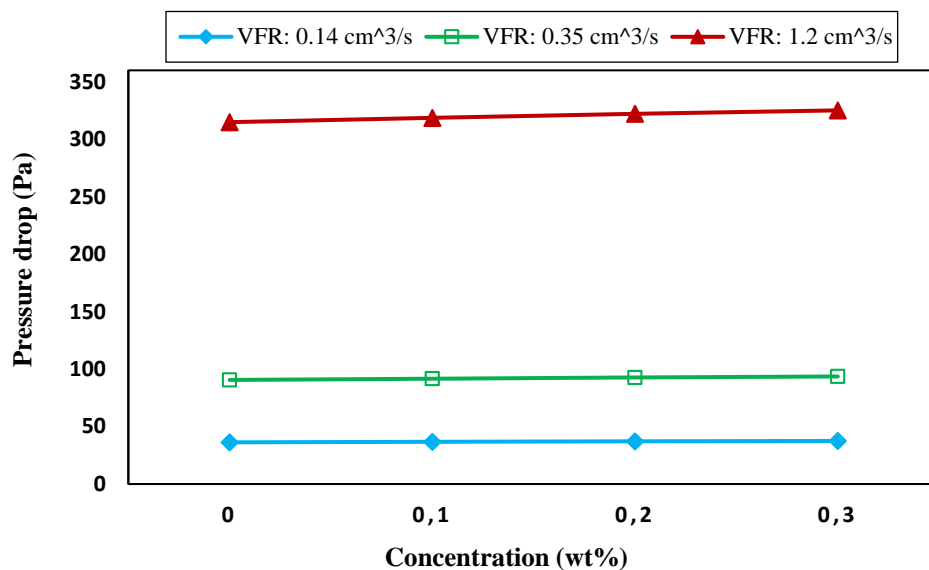
297

298

The maximum difference between the values of the pressure drop obtained from the simulation and the theoretical pressure drop is 1.75%, indicating acceptable accuracy of the simulation. According to figure 7 and Table 5, it can be seen that by increasing the concentration of TiO₂ nanoparticles at a given volume flow rate, the pressure drop increased due to the increased viscosity. As the concentration of the nanoparticles increases, the interaction between the nanoparticles increases, which also increases the viscosity. According to equation 5, the increment of viscosity can lead to an increase in pressure drop. To illustrate, by increasing the concentration from 0.1 to 0.3 wt% at a flow rate of $1.2 \frac{cm^3}{s}$, the pressure drop reached 318.65 Pa from 325.19 Pa. The higher the flow rates and the concentrations, the more pressure drop. The reason for this variation can be due to the insignificant change in viscosity at lower concentrations since nanoparticles could not affect the viscosity. Other scholars have indicated similar results in the experimental investigation [57, 58].

Figure 8 exhibits pressure drop variation of TiO₂ nanofluids at different volume flow rates. According to figure 8 and Table 5, it can be seen that as the flow rate increased, pressure drop increased for all concentrations, as it is followed by the fluid velocity increase and the direct

299 relationship of pressure drop with fluid velocity (equation 5). Additionally, considering
 300 equation 7, the Reynolds number is related to tube length, velocity, viscosity, and nanofluid
 301 density. Given the constant length of the tube and minor changes in viscosity and density, the
 302 leading cause of the pressure drop is related to an increase in flow rate. The highest pressure
 303 drop rate at any given concentration is related to the highest flow rate. For instance, by
 304 increasing the volume flow rate from 0.14 to $1.2 \frac{cm^3}{s}$, the pressure drop increased from 36.34
 305 Pa to 318.65 Pa for 0.1 wt% TiO₂ nanofluid; thus, the volume flow rate has a significant effect
 306 on the pressure drop. In a study conducted by Mousavi et al. [59], the pressure drop variations
 307 of the prepared nanofluids in a tube were investigated. Their findings were consistent with the
 308 modeling results.

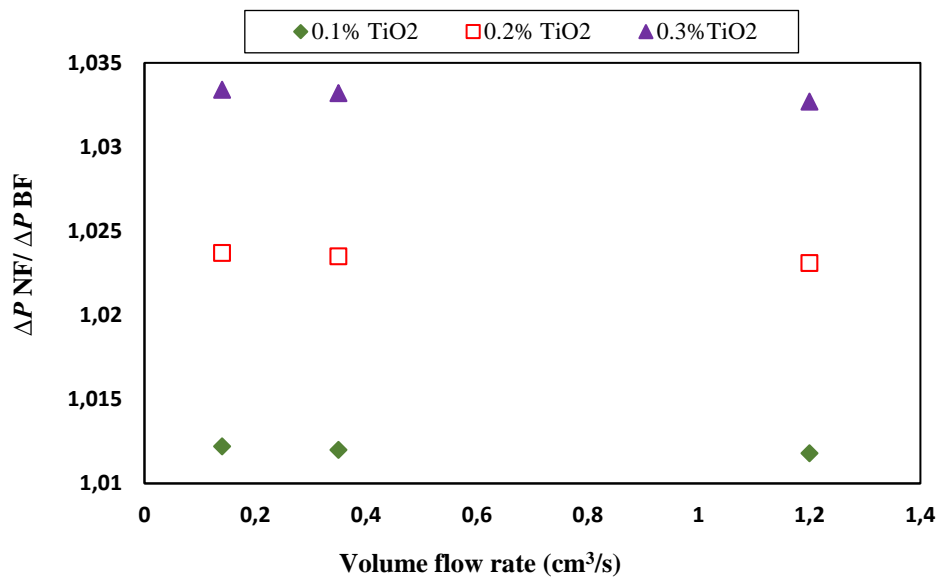


309

310 **Fig. 8.** Pressure drop variation of TiO₂ nanofluids at different volume flow rates.

311 Figure 9 represents the effect of volume flow rate on the pressure drop ratio of TiO₂
 312 nanofluids and pure oil. It can be seen that the increase in the volume flow rate of all prepared
 313 TiO₂ nanofluids led to a decrease in the pressure drop of the nanofluid to the base fluid. As the
 314 settling probability decreases; there will be a reduction in the high-volume flow rate, the ratio

315 of nanofluid pressure drop to base fluid pressure drop. By increasing the flow rate at the same
 316 concentration, the number of nanoparticles per volume was reduced, leading to a decrease in
 317 apparent viscosity. Also, this pressure drop ratio intensified with an increase in the
 318 concentration of nanoparticles at given volume flow rates. Pourfarhang et al. [65] studied the
 319 nanofluid flowing inside a car radiator and found that with increasing flow, the ratio of pressure
 320 drop to the base fluid decreases, and this result is consistent with the outputs of the simulation.



321

322 **Fig. 9.** Pressure drop ratio of TiO₂ nanofluids to base oil at different flow rates.

323 To investigate the coefficient of friction variations (Darcy's Weisbach coefficient of
 324 friction), the coefficient of friction of a pipe with a larger diameter was called F_1 . The
 325 coefficient of friction of a pipe with a smaller diameter was called F_2 . Table 6 is provided to
 326 compare the changes made on the coefficient of friction. Based on Table 6, the increase in the
 327 concentration of nanoparticles led to an increase in the coefficient of friction. At higher
 328 concentrations, the viscosity of the fluid and the coefficient of friction increased due to the
 329 agglomeration of nanoparticles. It is also apparent that as the volume flow rate increases, the
 330 coefficient of friction decreases since the coefficient of friction is inversely related to the fluid

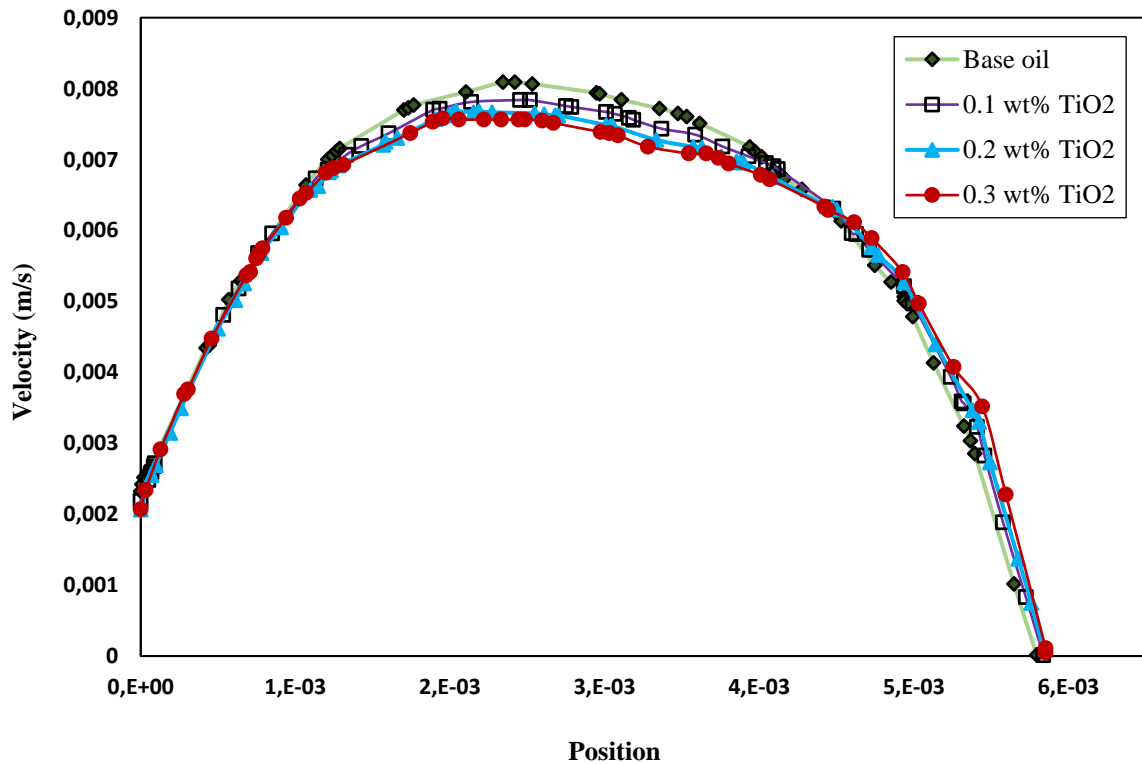
331 velocity (Eq. 5). Many researchers have also found that the coefficient of friction increases
 332 with the increasing concentration of nanoparticles and decreases with the increasing flow rate
 333 [1, 2, 59, 66].

334 **Table 6** Coefficient of friction at different concentrations and velocities of TiO₂ nanofluids.

Concentration (wt%)	Inlet velocity (m/s)	F_1	F_2
0 (base oil)	0.00483	45.88	31.37
	0.012	18.47	12.64
	0.0409	5.42	3.61
0.1 TiO ₂	0.00483	46.38	31.90
	0.012	18.67	12.78
	0.0409	5.48	3.78
0.2 TiO ₂	0.00483	46.89	32.00
	0.012	18.87	12.92
	0.0409	5.54	3.80
0.3 TiO ₂	0.00483	47.30	32.32
	0.012	19.04	13.03
	0.0409	5.59	3.83

335 Figure 10 shows the effect of adding TiO₂ nanoparticles on the velocity profile and reaching
 336 the fully developed state. It shows the state of the velocity profile at the tube's inlet for the base
 337 fluid and nanofluids containing 0.1, 0.2, and 0.3 wt% of TiO₂ nanoparticles at a volume flow
 338 rate of $0.14 \frac{cm^3}{s}$. In addition, with the addition of TiO₂ nanoparticles and increasing the
 339 concentration of nanoparticles, reaching the developed state occurs faster. Adding TiO₂
 340 nanoparticles led to an increase in viscosity; thus, considering equations 7 and 8, Reynolds

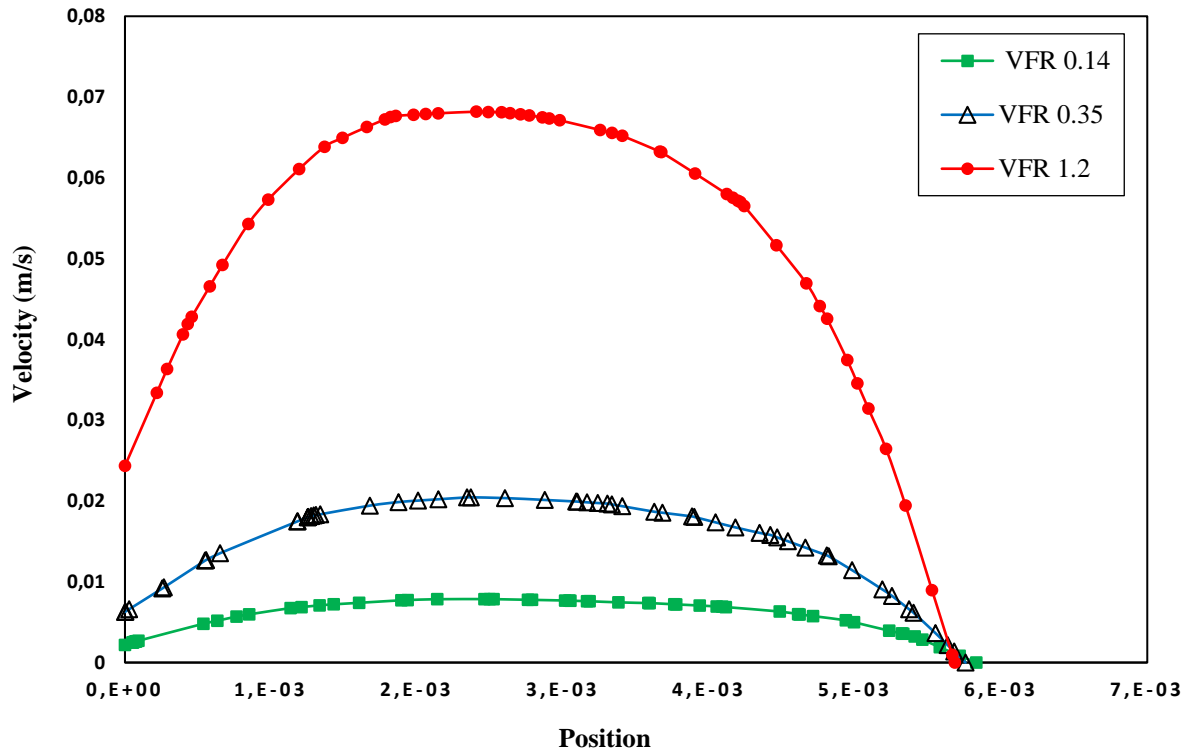
341 number and the entrance length decreased, and reaching the fully developed state occurred
342 faster.



343

344 **Fig. 10.** Velocity profile of TiO₂ nanofluids at pipe inlet at a volume flow rate of 0.14 ($\frac{cm^3}{s}$) and
345 different concentrations.

346 Figure 11 exhibits the effect of volume flow rate of 0.2 wt% TiO₂ nanofluid on the velocity
347 profile. It shows the velocity profile status at the inlet of the pipe containing 0.2 wt% of TiO₂
348 nanoparticles at different volume flow rates. It is observed that the increase of flow rate can
349 delay reaching the developed state. Because with increasing flow, the velocity increases, and
350 according to Equation 7, the Reynolds number increases. According to Equation 8, with
351 increasing Reynolds number, the entrance length increases, and reaching the fully developed
352 state is delayed. Gholinia et al. [67] examined the nanofluid flow inside a circular cylinder and
353 observed that increasing the velocity caused the development state to be delayed.



354

355 **Fig. 11.** Velocity profile of 0.2 wt% TiO₂ nanofluids at pipe inlet considering different volume
 356 flow rates.

357 **4.2. Results of MWCNTs/turbine meter oil nanofluid**

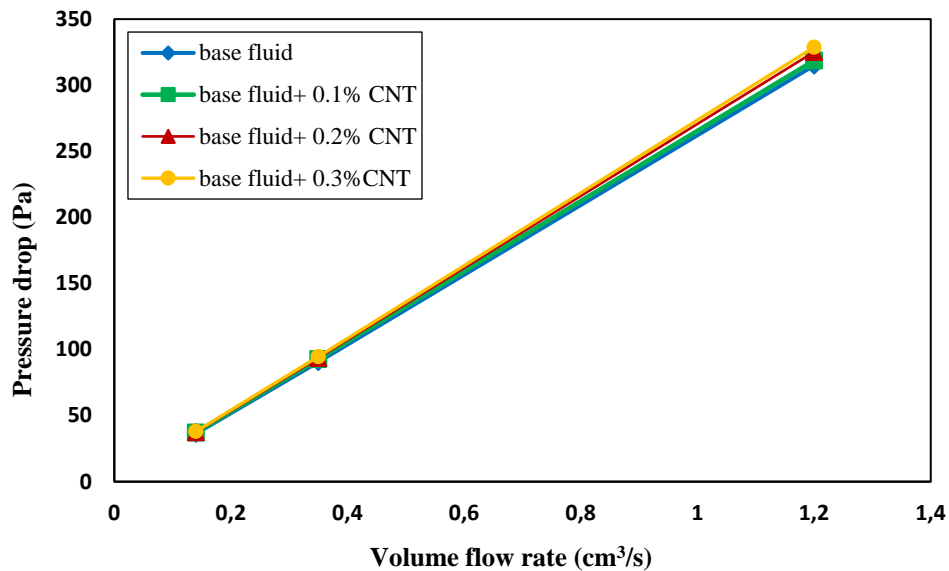
358 The effect of increasing the concentration of MWCNTs and volume flow rate on pressure
 359 drop, coefficient of friction, and velocity profile are discussed in this section. Moreover, the
 360 simultaneous effect of increasing the concentration of nanoparticles and volume flow rate on
 361 pressure drop are scrutinized.

362 Table 7 lists the pressure drop values of MWCNTs nanofluids at different volume flow
 363 rates. Figure 12 shows the effect of MWCNTs concentration on the variations of the pressure
 364 drop as a function of flow rate.

365

366 **Table 7** Modeling and theoretical pressure drop values of MWCNTs nanofluids at different flow
 367 rates.

Concentration (wt%)	Flow rate ($\frac{cm^3}{s}$)	Modeling pressure drop (Pa)	Theoretical pressure drop (Pa)	Difference (%)
0 (base oil)	0.14	36.28	36.44	0.439
	0.35	90.59	90.64	0.055
	1.2	314.91	310.74	1.342
0.1 MWCNTs	0.14	37.14	37.32	0.482
	0.35	92.72	92.80	0.086
	1.2	322.19	318.63	1.117
0.2 MWCNTs	0.14	37.47	37.68	0.557
	0.35	93.60	93.69	0.096
	1.2	325.18	319.81	1.679
0.3 MWCNTs	0.14	38.00	38.18	0.471
	0.35	94.64	94.65	0.010
	1.2	328.73	323.41	1.645



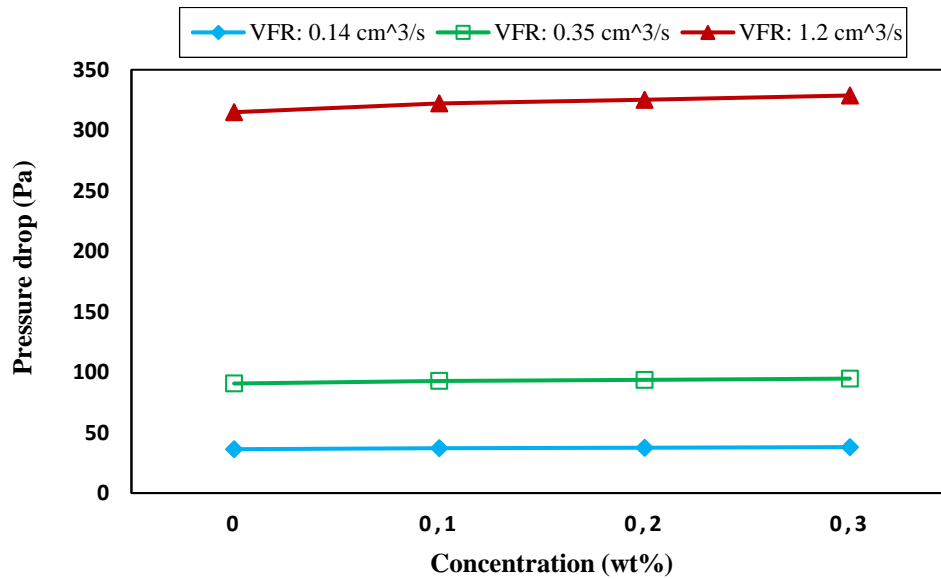
368

369 **Fig. 12.** The effect of MWCNTs concentration on the pressure drop variations as a function of

370 flow rate.

371 According to Figure 12 and Table 7, the pressure drop of the nanofluid can be increased by
372 increasing the concentration of MWCNTs at a given volume flow rate. The main reason for the
373 increased viscosity is that as the concentration of MWCNTs increases, the collision between
374 the MWCNTs increases because of increased random motion and increases viscosity. Due to
375 the direct relationship of pressure drop with a viscosity (Eq. 5), pressure drop at higher
376 percentages of MWCNTs shows a higher increase. At low concentrations of MWCNTs, the
377 upward pressure drop of nanofluid is much lower than that of high nanofluid concentrations.
378 In other words, at a low concentration of MWCNTs, the increase in pressure drop is not very
379 noticeable due to the unremarkable change in viscosity of nanofluids at low concentrations.

380 Figure 13 shows pressure drop variation of MWCNTs nanofluids at different volume flow
381 rates. According to Figure 13 and Table 7, it can be concluded that by increasing the volume
382 flow rate, the pressure drop increases, since the increase in volume flow rate results in an
383 increase in fluid velocity and the direct relationship between pressure drop and fluid velocity
384 (Eq. 5). To illustrate, at a 0.3 wt% concentration of MWCNTs, the pressure drop was raised
385 from 38 Pa to 94.64 Pa and then to 328.78 Pa. The results show the significant effect of
386 increasing discharge on increasing pressure drop. In a study conducted by Hussein et al. [57]
387 on a current-carrying nanofluid in a circular – mini - tube, they observed that with increasing
388 flow rate, the pressure drop increased, which was quite similar to the simulation results.



389

390

Fig. 13. Pressure drop variation of MWCNTs nanofluids at different volume flow rates.

391

392

393

394

395

396

397

398

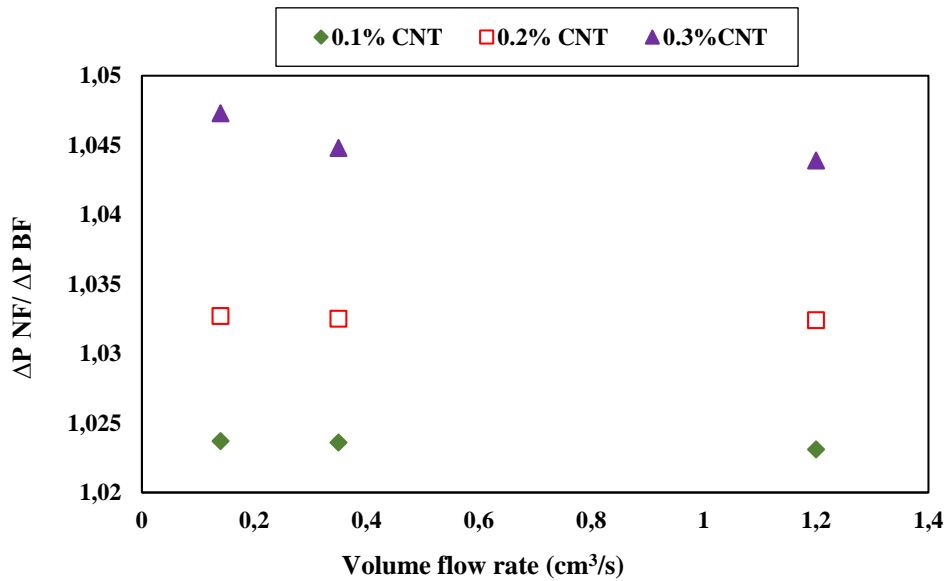
399

400

401

402

Figure 14 exhibits the effect of volume flow rate and concentration of MWCNTs on pressure drop. It can be seen that by increasing the volume flow rate at all concentrations, the pressure drop of nanofluids to the base fluids decreased. As the volume flow rate increased, the rate of fluid coalescence increased, and the fluid dispersion became uniform. Since nanoparticles' effect was the least at the lowest concentration, nanofluid properties were close to base fluid properties, and the lowest proportion of pressure drop could be seen at the lowest nanoparticle concentration and the highest volume flow rates. Moreover, the probability of sedimentation decreases with the trend. As a result of the high-volume flow rate, the pressure drop rate relative to the base fluid decreased. Therefore, using nanofluids in high volume flow rates will cause less pressure drop and be more appropriate. In the research of Pourfarhang et al. [65] and Naddaf et al. [58], it was observed that the pressure drop ratio of nanofluid to the base fluid decreased with increasing flow rate.



403

404

Fig. 14. Pressure drop ratio of MWCNTs nanofluids to base oil at different flow rates.

405

Table 8 lists the coefficient of frictions at different concentrations of MWCNTs nanofluids.

406

Considering Table 8, as the concentration of MWCNTs increased, the coefficient of friction

407

increased. It is also apparent that as the volume flow rate increased, the coefficient of friction

408

decreased because the coefficient of friction is inversely related to the fluid velocity (Eq. 5).

409

Figure 15 presents the effect of adding MWCNTs on the velocity profile and reaching the

410

fully developed state. It shows the status of the velocity profile at tube inlet for base fluid and

411

nanofluids containing 0.1, 0.2, and 0.3 wt% of MWCNTs at a volume flow rate of $0.35 \frac{cm^3}{s}$. As

412

can be seen, with the addition of MWCNTs and increasing the concentration of MWCNTs,

413

reaching the developed state can be faster. The Reynolds number decreased with the addition

414

of MWCNTs since they could increase the viscosity. According to Equation 8, with decreasing

415

Reynold number, the entrance length decreases and reaches the fully developed state. The same

416

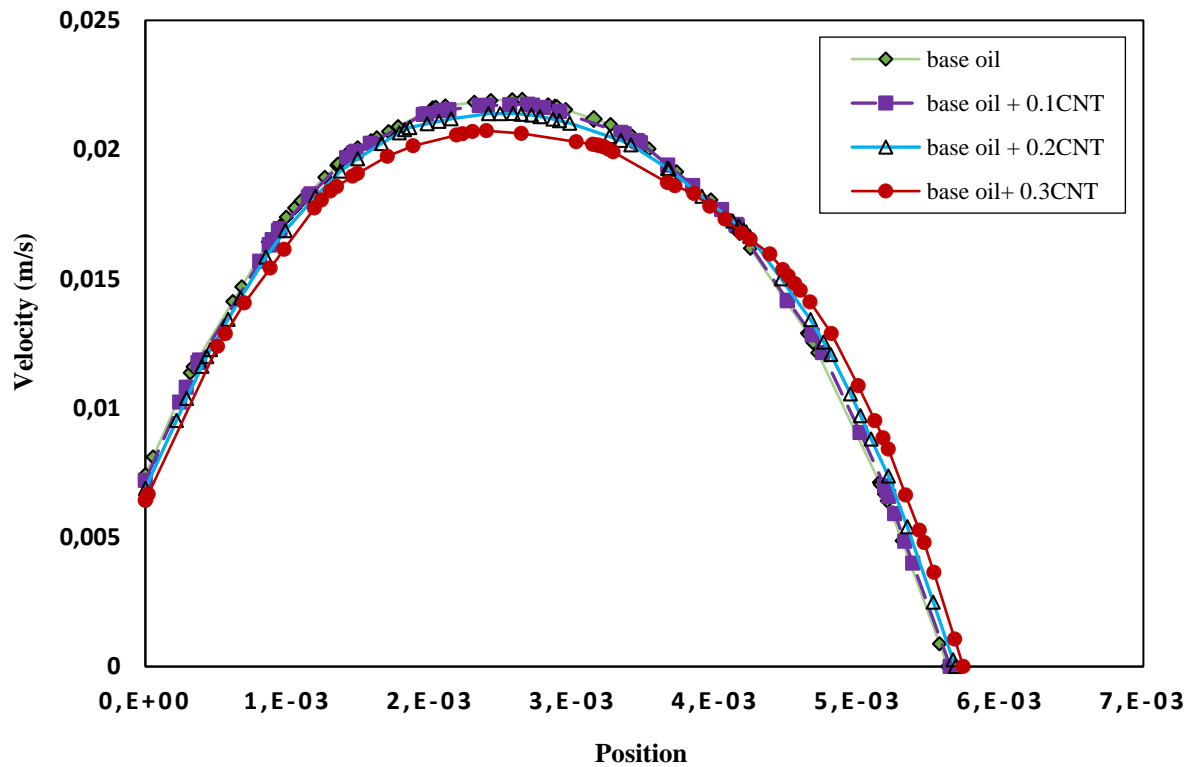
experimental results were reported in a study conducted by Bao et al. [68].

417

418

Table 8 Coefficient of friction at different concentrations and velocities of MWCNTs nanofluids.

Concentration (wt%)	Inlet velocity (m/s)	F_1	F_2
0 (base oil)	0.00483	45.88	31.37
	0.012	18.47	12.64
	0.0409	5.42	3.61
0.1 MWCNTs	0.00483	46.96	32.08
	0.012	18.89	12.78
	0.0409	5.54	3.80
0.2 MWCNTs	0.00483	47.34	32.36
	0.012	19.05	12.93
	0.0409	5.59	3.83
0.3 MWCNTs	0.00483	47.83	32.70
	0.012	19.25	13.18
	0.0409	5.65	3.87



421

422

Fig. 15. Velocity profile at pipe inlet at a volume flow rate of $0.35 \left(\frac{cm^3}{s}\right)$ and different

423

concentrations of MWCNTs.

424

Figure 16 shows the variations of the velocity profile at the inlet of the tube for nanofluids

425

containing 0.1, 0.2, and 0.3 wt% of MWCNTs at a volume flow rate of $0.35 \frac{cm^3}{s}$. Increasing

426

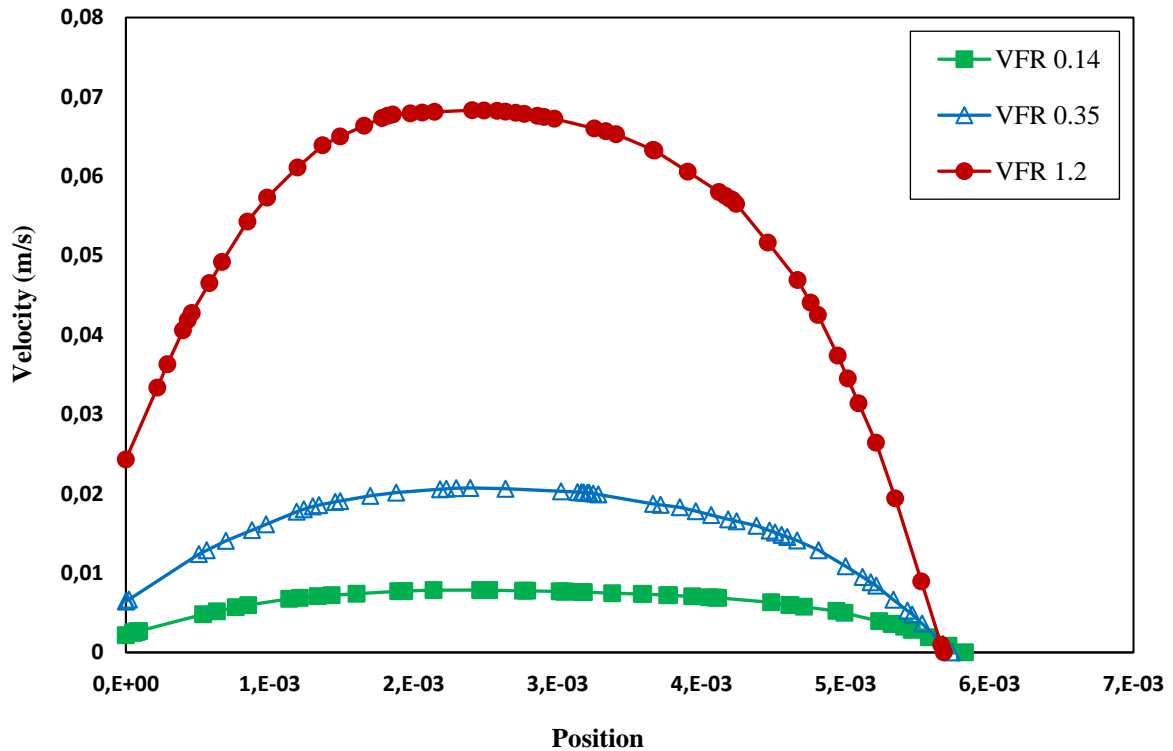
flow rate can delay the developed state because the velocity increases, and according to

427

Equation 7, the Reynolds number increases. According to Equation 8, with increasing Reynolds

428

number, the entrance length increases, and reaching the developed state is delayed.



429

430

Fig. 16. Velocity profile of 0.3 wt% MWCNTs nanofluids at different volume flow rates.

431

4.3. Comparison of the results of TiO₂ and MWCNTs nanofluids

432

433

434

435

436

437

438

439

440

Based on the acquired findings, it can be concluded that at a constant concentration of nanoparticles, the MWCNTs/turbine meter oil nanofluid had a higher pressure drop and friction coefficient than TiO₂/turbine meter oil nanofluid. This phenomenon occurred due to the larger dimensions of MWCNTs (13 nm) than the TiO₂ nanoparticles (10 nm). The number of particles in the nanofluid containing MWCNTs was greater than the nanofluid containing TiO₂ nanoparticles. Thus, increasing these particles' movement and random motion increased the pressure drop of MWCNTs/turbine meter oil nanofluid. Additionally, due to the shape of the MWCNTs, they were more likely to be agglomerated and be more viscous; accordingly, they increased the pressure drop and coefficient of friction.

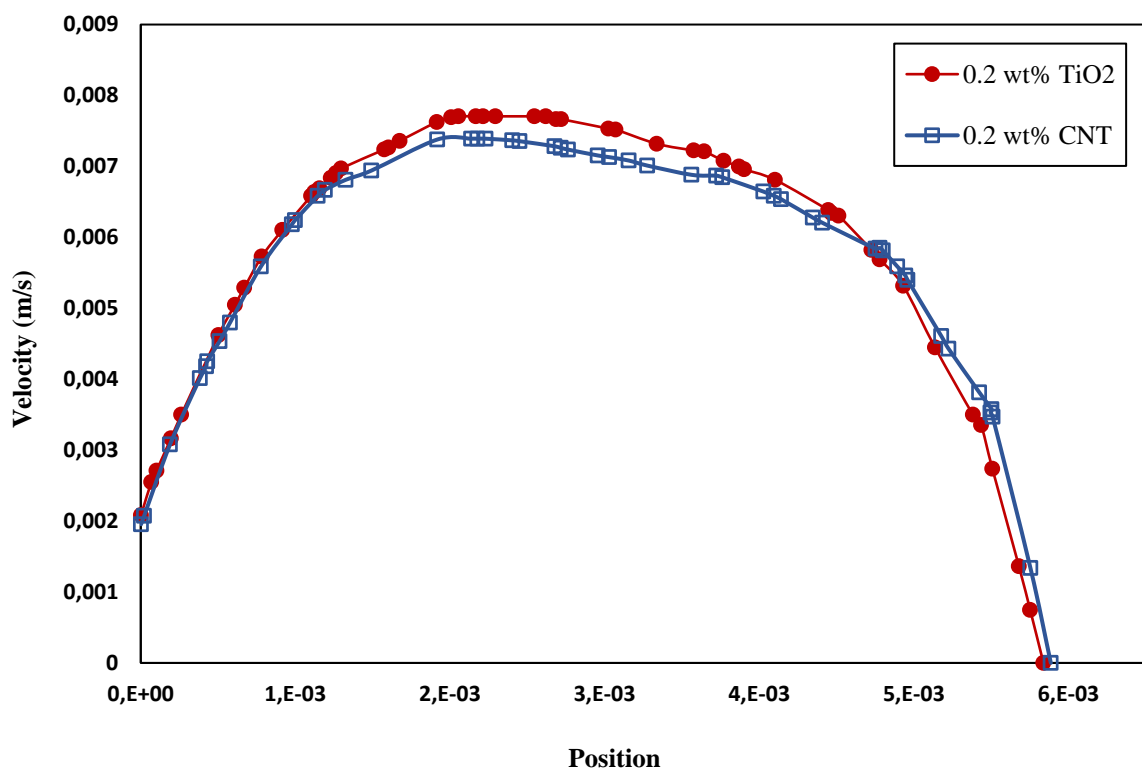
441

442

Figure 17 shows the velocity profile of nanofluids containing TiO₂ and MWCNTs at different positions. It is observed that nanofluids containing MWCNTs developed faster than

443 nanofluids containing TiO₂. Since the viscosity of MWCNTs/turbine meter oil was higher than
444 that of TiO₂/turbine meter oil, the Reynolds number was further reduced and developed faster.

445 Toghraei et al. [69] simulated the flow of a fluid containing platinum and copper
446 nanoparticles into a nanochannel. They reported that since the size of platinum particles was
447 larger than copper, the nanofluid containing platinum developed faster.



448
449 **Fig. 17.** Velocity profile of 0.2 wt% TiO₂ and MWCNTs nanofluids at a flow rate of 0.14

450 $\frac{cm^3}{s}$ at different positions.

451 5. Conclusion

452 This simulation aimed to investigate the effect of MWCNTs and TiO₂ nanoparticles on the
453 performance of the gas turbine meter oil. Moreover, the pressure drop and coefficient of friction
454 of TiO₂/turbine meter oil and MWCNTs/turbine meter oil nanofluids were studied.

455 With the increase of concentration of nanoparticles, the pressure drop increased due to the
456 higher viscosity of the prepared nanofluids at higher concentrations. Furthermore, As the
457 volume flow rate increased, the nanofluid pressure drop increased. It was further observed that
458 the coefficient of friction increased with the increase of nanoparticles concentration at a
459 constant volume flow rate. Considering each nanofluid, it was concluded that the coefficient
460 of friction was inversely related to the volume flow rate. Concerning the physical
461 characteristics of the pipe, it was reported that at higher concentrations of nanoparticles, a faster
462 fully developed state occurred. Moreover, the MWCNTs/turbine meter oil nanofluids
463 represented a higher coefficient of friction and pressure drops compared to the TiO₂/turbine
464 meter oil nanofluid.

465 **Author contribution:**

466 **Atiyeh Aghaei Sarvari:** Investigation, Methodology, Conceptualization, Formal analysis,
467 Writing original draft. **Saeed Zeinali Heris:** Supervision, Conceptualization, Formal analysis,
468 Validation, Review & Editing. **Mousa Mohammadpourfard:**, Review & Editing. **Seyed**
469 **Borhan Mousavi:**, Formal analysis, Writing original draft. **Patrice Estellé:** Validation,
470 Review & Editing.

471 **6. References**

- 472 [1] S. B. Mousavi, S. Z. Heris, and P. Estellé, "Experimental comparison between ZnO and
473 MoS₂ nanoparticles as additives on performance of diesel oil-based nano lubricant,"
474 *Scientific reports*, vol. 10, no. 1, pp. 1-17, 2020.
- 475 [2] S. B. Mousavi, S. Z. Heris, and P. Estellé, "Viscosity, tribological and physicochemical
476 features of ZnO and MoS₂ diesel oil-based nanofluids: An experimental study," *Fuel*,
477 vol. 293, p. 120481, 2021.

- 478 [3] Y. Singh, A. Sharma, N. K. Singh, and M. Noor, "Effect of SiC nanoparticles
479 concentration on novel feedstock Moringa Oleifera chemically treated with
480 neopentylglycol and their tribological behavior," *Fuel*, vol. 280, p. 118630, 2020.
- 481 [4] A. Boroomandpour, D. Toghraie, and M. Hashemian, "A comprehensive experimental
482 investigation of thermal conductivity of a ternary hybrid nanofluid containing
483 MWCNTs-titania-zinc oxide/water-ethylene glycol (80: 20) as well as binary and mono
484 nanofluids," *Synthetic Metals*, vol. 268, p. 116501, 2020.
- 485 [5] D. Toghraie, N. Sina, N. A. Jolfaei, M. Hajian, and M. Afrand, "Designing an Artificial
486 Neural Network (ANN) to predict the viscosity of Silver/Ethylene glycol nanofluid at
487 different temperatures and volume fraction of nanoparticles," *Physica A: Statistical
488 Mechanics and its Applications*, vol. 534, p. 122142, 2019.
- 489 [6] P. Barnoon, D. Toghraie, F. Eslami, and B. Mehmandoust, "Entropy generation
490 analysis of different nanofluid flows in the space between two concentric horizontal
491 pipes in the presence of magnetic field: single-phase and two-phase approaches,"
492 *Computers & Mathematics with Applications*, vol. 77, no. 3, pp. 662-692, 2019.
- 493 [7] F. T. Hong, A. Schneider, and S. M. Sarathy, "Enhanced lubrication by core-shell TiO₂
494 nanoparticles modified with gallic acid ester," *Tribology International*, vol. 146, p.
495 106263, 2020.
- 496 [8] A. Samadzadeh and S. Z. Heris, "Effect of stabilization method on the natural
497 convection in an inclined cavity filled with MWCNTs/water nanofluids," *International
498 Communications in Heat and Mass Transfer*, vol. 129, p. 105645, 2021.
- 499 [9] A. Samadzadeh, S. Z. Heris, I. Hashim, and O. Mahian, "An experimental investigation
500 on natural convection of non-covalently functionalized MWCNTs nanofluids: effects
501 of aspect ratio and inclination angle," *International Communications in Heat and Mass
502 Transfer*, vol. 111, p. 104473, 2020.

- 503 [10] S. Z. Heris, M. Fallahi, M. Shanbedi, and A. Amiri, "Heat transfer performance of two-
504 phase closed thermosyphon with oxidized CNT/water nanofluids," *Heat and Mass*
505 *Transfer*, vol. 52, no. 1, pp. 85-93, 2016.
- 506 [11] M. H. Aghahadi, M. Niknejadi, and D. Toghraie, "An experimental study on the
507 rheological behavior of hybrid Tungsten oxide (WO₃)-MWCNTs/engine oil
508 Newtonian nanofluids," *Journal of Molecular Structure*, vol. 1197, pp. 497-507, 2019.
- 509 [12] F. Soltani, D. Toghraie, and A. Karimipour, "Experimental measurements of thermal
510 conductivity of engine oil-based hybrid and mono nanofluids with tungsten oxide
511 (WO₃) and MWCNTs inclusions," *Powder Technology*, vol. 371, pp. 37-44, 2020.
- 512 [13] P. Sreedevi and P. S. Reddy, "Entropy generation and heat transfer analysis of alumina
513 and carbon nanotubes based hybrid nanofluid inside a cavity," *Physica Scripta*, vol. 96,
514 no. 8, p. 085210, 2021.
- 515 [14] M. Doğan, A. Selek, O. Turhan, B. K. Kızılduman, and Z. Bicil, "Different functional
516 groups functionalized hexagonal boron nitride (h-BN) nanoparticles and multi-walled
517 carbon nanotubes (MWCNT) for hydrogen storage," *Fuel*, vol. 303, p. 121335, 2021.
- 518 [15] E. M. C. Contreras and E. P. Bandarra Filho, "HEAT TRANSFER PERFORMANCE
519 OF AN AUTOMOTIVE RADIATOR WITH MWCNT NANOFLUID COOLING IN
520 A HIGH OPERATING TEMPERATURE RANGE," *Applied Thermal Engineering*, p.
521 118149, 2022.
- 522 [16] Z. Said, P. Sharma, L. S. Sundar, A. Afzal, and C. Li, "Synthesis, stability,
523 thermophysical properties and AI approach for predictive modelling of Fe₃O₄ coated
524 MWCNT hybrid nanofluids," *Journal of Molecular Liquids*, vol. 340, p. 117291, 2021.
- 525 [17] W. He *et al.*, "Using of artificial neural networks (ANNs) to predict the thermal
526 conductivity of zinc oxide–silver (50%–50%)/water hybrid Newtonian nanofluid,"
527 *International Communications in Heat and Mass Transfer*, vol. 116, p. 104645, 2020.

- 528 [18] S.-R. Yan, D. Toghraie, L. A. Abdulkareem, A. a. Alizadeh, P. Barnoon, and M.
529 Afrand, "The rheological behavior of MWCNTs–ZnO/Water–Ethylene glycol hybrid
530 non-Newtonian nanofluid by using of an experimental investigation," *Journal of*
531 *Materials Research and Technology*, vol. 9, no. 4, pp. 8401-8406, 2020.
- 532 [19] S. Rostami, D. Toghraie, B. Shabani, N. Sina, and P. Barnoon, "Measurement of the
533 thermal conductivity of MWCNT-CuO/water hybrid nanofluid using artificial neural
534 networks (ANNs)," *Journal of Thermal Analysis and Calorimetry*, vol. 143, no. 2, pp.
535 1097-1105, 2021.
- 536 [20] P. S. Reddy and P. Sreedevi, "Flow and heat transfer analysis of carbon nanotubes based
537 nanofluid flow inside a cavity with modified Fourier heat flux," *Physica Scripta*, vol.
538 96, no. 5, p. 055215, 2021.
- 539 [21] P. S. Reddy, P. Sreedevi, and K. V. S. Rao, "Impact of heat generation/absorption on
540 heat and mass transfer of nanofluid over rotating disk filled with carbon nanotubes,"
541 *International Journal of Numerical Methods for Heat & Fluid Flow*, 2020.
- 542 [22] P. Sreedevi and P. Sudarsana Reddy, "Impact of Convective Boundary Condition on
543 Heat and Mass Transfer of Nanofluid Flow Over a Thin Needle Filled with Carbon
544 Nanotubes," *Journal of Nanofluids*, vol. 9, no. 4, pp. 282-292, 2020.
- 545 [23] P. Sudarsana Reddy, K. Jyothi, and M. Suryanarayana Reddy, "Flow and heat transfer
546 analysis of carbon nanotubes-based Maxwell nanofluid flow driven by rotating
547 stretchable disks with thermal radiation," *Journal of the Brazilian Society of*
548 *Mechanical Sciences and Engineering*, vol. 40, no. 12, pp. 1-16, 2018.
- 549 [24] Z. S. Mahmoudabadi, A. Rashidi, and A. Tavasoli, "Synthesis of two-dimensional
550 TiO₂@ multi-walled carbon nanotube nanocomposites as smart nanocatalyst for ultra-
551 deep oxidative desulfurization of liquid fuel: Optimization via response surface
552 methodology," *Fuel*, vol. 306, p. 121635, 2021.

- 553 [25] Y. Singh, D. Singh, A. Singla, A. Sharma, and N. K. Singh, "Chemical modification of
554 juliflora oil with trimethylolpropane (TMP) and effect of TiO₂ nanoparticles
555 concentration during tribological investigation," *Fuel*, vol. 280, p. 118704, 2020.
- 556 [26] M. Valihesari, V. Pirouzfard, F. Ommi, and F. Zamankhan, "Investigating the effect of
557 Fe₂O₃ and TiO₂ nanoparticle and engine variables on the gasoline engine performance
558 through statistical analysis," *Fuel*, vol. 254, p. 115618, 2019.
- 559 [27] J. Hou, H. Yang, B. He, J. Ma, Y. Lu, and Q. Wang, "High photocatalytic performance
560 of hydrogen evolution and dye degradation enabled by CeO₂ modified TiO₂ nanotube
561 arrays," *Fuel*, vol. 310, p. 122364, 2022.
- 562 [28] B. Ruhani, P. Barnoon, and D. Toghraie, "Statistical investigation for developing a new
563 model for rheological behavior of Silica–ethylene glycol/Water hybrid Newtonian
564 nanofluid using experimental data," *Physica A: Statistical Mechanics and Its
565 Applications*, vol. 525, pp. 616-627, 2019.
- 566 [29] P. Sreedevi and P. S. Reddy, "Effect of magnetic field and thermal radiation on natural
567 convection in a square cavity filled with TiO₂ nanoparticles using Tiwari-Das nanofluid
568 model," *Alexandria Engineering Journal*, vol. 61, no. 2, pp. 1529-1541, 2022.
- 569 [30] S. Rostami, S. Mahdavi, M. Alinezhadfar, and A. Mohseni, "Tribological and corrosion
570 behavior of electrochemically deposited Co/TiO₂ micro/nano-composite coatings,"
571 *Surface and Coatings Technology*, vol. 423, p. 127591, 2021.
- 572 [31] W. H. Kan and L. Chang, "The mechanisms behind the tribological behaviour of
573 polymer matrix composites reinforced with TiO₂ nanoparticles," *Wear*, vol. 474, p.
574 203754, 2021.
- 575 [32] M. S. Park, C. S. Lee, J. H. Lee, D. Y. Ryu, and J. H. Kim, "Dissolution–precipitation
576 approach for long-term stable low-friction composites consisting of mesoporous TiO₂

- 577 nanospheres and carbon black in Poly (Vinylidene fluoride) matrix," *Tribology*
578 *International*, vol. 145, p. 106187, 2020.
- 579 [33] A. Shahsavari, S. Khanmohammadi, D. Toghraie, and H. Salihepour, "Experimental
580 investigation and develop ANNs by introducing the suitable architectures and training
581 algorithms supported by sensitivity analysis: measure thermal conductivity and
582 viscosity for liquid paraffin based nanofluid containing Al₂O₃ nanoparticles," *Journal*
583 *of Molecular Liquids*, vol. 276, pp. 850-860, 2019.
- 584 [34] I. Ali *et al.*, "Advances in carbon nanomaterials as lubricants modifiers," *Journal of*
585 *molecular liquids*, vol. 279, pp. 251-266, 2019.
- 586 [35] Y. Singh, N. K. Singh, A. Sharma, A. Singla, D. Singh, and E. Abd Rahim, "Effect of
587 ZnO nanoparticles concentration as additives to the epoxidized Euphorbia Lathyris oil
588 and their tribological characterization," *Fuel*, vol. 285, p. 119148, 2021.
- 589 [36] M. Heidari, M. Tahmasebpour, A. Antzaras, and A. A. Lemonidou, "CO₂ capture and
590 fluidity performance of CaO-based sorbents: Effect of Zr, Al and Ce additives in tri-,
591 bi-and mono-metallic configurations," *Process Safety and Environmental Protection*,
592 vol. 144, pp. 349-365, 2020.
- 593 [37] M. Heidari, M. Tahmasebpour, S. B. Mousavi, and C. Pevida, "CO₂ capture activity of
594 a novel CaO adsorbent stabilized with (ZrO₂+ Al₂O₃+ CeO₂)-based additive under
595 mild and realistic calcium looping conditions," *Journal of CO₂ Utilization*, vol. 53, p.
596 101747, 2021.
- 597 [38] S. S. Seyedi, M. R. Shabgard, S. B. Mousavi, and S. Z. Heris, "The impact of SiC,
598 Al₂O₃, and B₂O₃ abrasive particles and temperature on wear characteristics of 18Ni
599 (300) maraging steel in abrasive flow machining (AFM)," *International Journal of*
600 *Hydrogen Energy*, 2021.

- 601 [39] Y. Singh and E. Abd Rahim, "Michelia Champaca: Sustainable novel non-edible oil as
602 nano based bio-lubricant with tribological investigation," *fuel*, vol. 282, p. 118830,
603 2020.
- 604 [40] S. K. Chaurasia, N. K. Singh, and L. K. Singh, "Friction and wear behavior of
605 chemically modified Sal (Shorea Robusta) oil for bio based lubricant application with
606 effect of CuO nanoparticles," *fuel*, vol. 282, p. 118762, 2020.
- 607 [41] B. A. Vardhaman, M. Amarnath, J. Ramkumar, and K. Mondal, "Enhanced tribological
608 performances of zinc oxide/MWCNTs hybrid nanomaterials as the effective lubricant
609 additive in engine oil," *Materials Chemistry and Physics*, vol. 253, p. 123447, 2020.
- 610 [42] B. Wang, Q. Fu, L. Sun, Y. Lu, and Y. Liu, "Improving the tribological performance of
611 carbon fiber reinforced resin composite by grafting MWCNT and GNPs on fiber
612 surface," *Materials Letters*, vol. 306, p. 130953, 2022.
- 613 [43] C. Almeida *et al.*, "Experimental Studies on Thermophysical and Electrical Properties
614 of Graphene–Transformer Oil Nanofluid," *Fluids*, vol. 5, no. 4, p. 172, 2020.
- 615 [44] H. Akbarpour, A. Rashidi, M. Mirjalili, and A. Nazari, "Comparison of the conductive
616 properties of polyester/viscose fabric treated with Cu nanoparticle and MWCNT s,"
617 *Journal of Nanostructure in Chemistry*, vol. 9, no. 4, pp. 335-348, 2019.
- 618 [45] A. S. Al-Janabi, M. Hussin, and M. Abdullah, "Stability, thermal conductivity and
619 rheological properties of graphene and MWCNT in nanolubricant using additive
620 surfactants," *Case Studies in Thermal Engineering*, vol. 28, p. 101607, 2021.
- 621 [46] H. Rangaswamy, M. P. G. Chandrashekarappa, D. Y. Pimenov, K. Giasin, and S.
622 Wojciechowski, "Experimental investigation and optimization of compression
623 moulding parameters for MWCNT/glass/kevlar/epoxy composites on mechanical and
624 tribological properties," *journal of materials research and technology*, vol. 15, pp. 327-
625 341, 2021.

- 626 [47] M. Padhan, U. Marathe, and J. Bijwe, "Tribology of Poly (etherketone) composites
627 based on nano-particles of solid lubricants," *Composites Part B: Engineering*, p.
628 108323, 2020.
- 629 [48] R. de la Cruz Parejas, F. J. Moura, R. R. de Avillez, and P. R. de Souza Mendes, "Effects
630 of Al₂O₃-NiO, TiO₂ and (Mg, Ni) O particles on the viscosity of heavy oil during
631 aquathermolysis," *Colloids and Surfaces A: Physicochemical and Engineering Aspects*,
632 vol. 625, p. 126863, 2021.
- 633 [49] A. M. Abdullah *et al.*, "Tailoring the viscosity of water and ethylene glycol based TiO₂
634 nanofluids," *Journal of Molecular Liquids*, vol. 297, p. 111982, 2020.
- 635 [50] V. V. Wanatasanapan, M. Abdullah, and P. Gunnasegaran, "Effect of TiO₂-Al₂O₃
636 nanoparticle mixing ratio on the thermal conductivity, rheological properties, and
637 dynamic viscosity of water-based hybrid nanofluid," *Journal of Materials Research
638 and Technology*, vol. 9, no. 6, pp. 13781-13792, 2020.
- 639 [51] S. Z. Heris, F. Farzin, and H. Sardarabadi, "Experimental comparison among thermal
640 characteristics of three metal oxide nanoparticles/turbine oil-based nanofluids under
641 laminar flow regime," *International Journal of Thermophysics*, vol. 36, no. 4, pp. 760-
642 782, 2015.
- 643 [52] M. Hosseinzadeh, S. Z. Heris, A. Beheshti, and M. Shanbedi, "Convective heat transfer
644 and friction factor of aqueous Fe₃O₄ nanofluid flow under laminar regime," *Journal
645 of Thermal Analysis and Calorimetry*, vol. 124, no. 2, pp. 827-838, 2016.
- 646 [53] M. K. A. Ali, H. Xianjun, R. F. Turkson, Z. Peng, and X. Chen, "Enhancing the
647 thermophysical properties and tribological behaviour of engine oils using nano-
648 lubricant additives," *RSC advances*, vol. 6, no. 81, pp. 77913-77924, 2016.

- 649 [54] F. L. G. Borda, S. J. R. de Oliveira, L. M. S. M. Lazaro, and A. J. K. Leiróz,
650 "Experimental investigation of the tribological behavior of lubricants with additive
651 containing copper nanoparticles," *Tribology International*, vol. 117, pp. 52-58, 2018.
- 652 [55] M. Laad and V. K. S. Jatti, "Titanium oxide nanoparticles as additives in engine oil,"
653 *Journal of King Saud University-Engineering Sciences*, vol. 30, no. 2, pp. 116-122,
654 2018.
- 655 [56] F. Curà, A. Mura, and F. Adamo, "Experimental investigation about tribological
656 performance of grapheme-nanoplatelets as additive for lubricants," *Procedia Structural
657 Integrity*, vol. 12, pp. 44-51, 2018.
- 658 [57] A. A. Hussien, N. M. Yusop, M. Z. Abdullah, A.-N. Moh'd A, and M. Khavarian,
659 "Study on convective heat transfer and pressure drop of MWCNTs/water nanofluid in
660 mini-tube," *Journal of Thermal Analysis and Calorimetry*, vol. 135, no. 1, pp. 123-132,
661 2019.
- 662 [58] A. Naddaf, S. Z. Heris, and B. Pouladi, "An experimental study on heat transfer
663 performance and pressure drop of nanofluids using graphene and multi-walled carbon
664 nanotubes based on diesel oil," *Powder Technology*, vol. 352, pp. 369-380, 2019.
- 665 [59] S. B. Mousavi, S. Z. Heris, and M. G. Hosseini, "Experimental investigation of
666 MoS₂/diesel oil nanofluid thermophysical and rheological properties," *International
667 Communications in Heat and Mass Transfer*, vol. 108, p. 104298, 2019.
- 668 [60] R. K. Ajeel and W.-I. Salim, "Experimental assessment of heat transfer and pressure
669 drop of nanofluid as a coolant in corrugated channels," *Journal of Thermal Analysis
670 and Calorimetry*, pp. 1-13, 2020.
- 671 [61] H. Pourpasha, S. Z. Heris, O. Mahian, and S. Wongwises, "The effect of multi-wall
672 carbon nanotubes/turbine meter oil nanofluid concentration on the thermophysical
673 properties of lubricants," *Powder Technology*, vol. 367, pp. 133-142, 2020.

- 674 [62] E. S. Menon, *Working Guide to Pump and Pumping Stations: Calculations and*
675 *Simulations*. Gulf Professional Publishing, 2009.
- 676 [63] M. Kutz, *Mechanical Engineers' Handbook, Volume 4: Energy and Power*. John Wiley
677 & Sons, 2015.
- 678 [64] M. Everts and J. P. Meyer, "Laminar hydrodynamic and thermal entrance lengths for
679 simultaneously hydrodynamically and thermally developing forced and mixed
680 convective flows in horizontal tubes," *Experimental Thermal and Fluid Science*, vol.
681 118, p. 110153, 2020.
- 682 [65] P. Samira, Z. H. Saeed, S. Motahare, and K. Mostafa, "Pressure drop and thermal
683 performance of CuO/ethylene glycol (60%)-water (40%) nanofluid in car radiator,"
684 *Korean journal of chemical engineering*, vol. 32, no. 4, pp. 609-616, 2015.
- 685 [66] S. B. Mousavi and S. Z. Heris, "Experimental investigation of ZnO nanoparticles
686 effects on thermophysical and tribological properties of diesel oil," *International*
687 *Journal of Hydrogen Energy*, vol. 45, no. 43, pp. 23603-23614, 2020.
- 688 [67] M. Gholinia, S. Gholinia, K. Hosseinzadeh, and D. Ganji, "Investigation on ethylene
689 glycol nano fluid flow over a vertical permeable circular cylinder under effect of
690 magnetic field," *Results in Physics*, vol. 9, pp. 1525-1533, 2018.
- 691 [68] L. Bao, C. Zhong, P. Jie, and Y. Hou, "The effect of nanoparticle size and nanoparticle
692 aggregation on the flow characteristics of nanofluids by molecular dynamics
693 simulation," *Advances in Mechanical Engineering*, vol. 11, no. 11, p.
694 1687814019889486, 2019.
- 695 [69] D. Toghraie, M. Mokhtari, and M. Afrand, "Molecular dynamic simulation of copper
696 and platinum nanoparticles Poiseuille flow in a nanochannels," *Physica E: Low-*
697 *dimensional Systems and Nanostructures*, vol. 84, pp. 152-161, 2016.
- 698